

## Scanning tunneling microscopy currents on locally disordered graphene

N. M. R. Peres,<sup>1</sup> Shan-Wen Tsai,<sup>2</sup> J. E. Santos,<sup>1</sup> and R. M. Ribeiro<sup>1</sup>

<sup>1</sup>*Department of Physics and Center of Physics, Universidade do Minho, P-4710-057 Braga, Portugal*

<sup>2</sup>*Department of Physics and Astronomy, University of California, Riverside, California 92521, USA*

(Received 6 February 2009; revised manuscript received 13 March 2009; published 27 April 2009)

We study the local density of states at and around a substituting impurity, and use these results to compute current versus bias characteristic curves of scanning tunneling microscopy (STM) experiments done on the surface of graphene. This allows us to detect the presence of substituting impurities on graphene. The case of vacancies is also analyzed. We find that the shape and magnitude of the STM characteristic curves depend on the position of the tip and on the nature of the defect, with the strength of the binding between the impurity and the carbon atoms playing an important role. Also the nature of the last atom of the tip has an influence on the shape of the characteristic curve.

DOI: [10.1103/PhysRevB.79.155442](https://doi.org/10.1103/PhysRevB.79.155442)

PACS number(s): 81.05.Uw, 73.20.Hb, 73.23.-b, 68.37.Ef

### I. INTRODUCTION

Graphene<sup>1,2</sup> consists of a monolayer of carbon atoms forming a two-dimensional honeycomb lattice. It has been intensively studied due to its fascinating physical properties<sup>3</sup> and potential applications. The honeycomb lattice consists of two triangular sublattices, and this is responsible for the linear dispersion of the low-energy excitations and for a pseudospin degree of freedom for electrons in graphene. Many of the novel properties of graphene follow from these two facts. Because of the Dirac spectrum, disorder can have a significant effect on the electronic properties of graphene, the effect being especially strong when the chemical potential crosses the Dirac point. Extrinsic disorder in graphene can be in the form of impurities,<sup>4–8</sup> topological defects,<sup>9–12</sup> edges,<sup>13,14</sup> and substrate corrugations.<sup>15</sup> In addition, there is also disorder in the form of intrinsic ripples in the structure of graphene.<sup>16–18</sup> Disorder in graphene occurs naturally but can also be induced if this is advantageous, tailoring its transport properties. This is the case for the recently produced material graphene.<sup>19</sup> Among the several possibilities, the replacement of a carbon atom by a different atom can occur. Atomic substitution in a carbon honeycomb lattice is chemically possible for boron (B) and nitrogen (N) atoms. There have been several experimental studies of B and N substitutions in highly oriented pyrolytic graphite,<sup>20,21</sup> graphitic structures,<sup>22</sup> and nanoribbons.<sup>23</sup>

In a previous publication<sup>24</sup> the problem of chemical substitution in graphene has been considered, and the local density of states (LDOS) and local electronic structure and charge distribution have been numerically calculated. In this work, we extend the calculation of the spatial dependence of the LDOS at and around the impurity using analytical methods, and extending the calculations for energies way beyond the Dirac point, an essential ingredient for the calculation of scanning tunneling microscopy (STM) currents at finite bias. Using these results we perform theoretical calculations of the tunneling current versus bias characteristic curves of STM studies on graphene surfaces with dilute substitution impurities. The STM technique is one of the most powerful tools for studying surfaces. This is particularly convenient for the study of graphene, which is two dimensional and exposed to

the STM tip. There have been several STM studies of both graphene grown epitaxially on SiC,<sup>25–27</sup> and mechanically exfoliated graphene on SiO<sub>2</sub>.<sup>15,28–31</sup> Our results can be used to interpret the STM signal when the tip comes close to a substituting impurity. A related study, computing the LDOS for point defects in graphene, using first-principles methods, was recently performed.<sup>32</sup> A study of the LDOS starting from the Dirac equation considering the effect of magnetic impurities was also recently considered.<sup>33</sup> The effect of local potentials with finite strength was studied in Ref. 34.

In Sec. II we present the tight-binding model and the Green's function formalism used. For a single localized substitutional impurity, the Green's function can be obtained exactly in closed analytical form. In Sec. III we discuss results for the LDOS and in Sec. IV the results for the tunneling current are presented. Section V contain further discussions and conclusions.

### II. CALCULATION OF THE GREEN'S FUNCTION FOR DISORDERED GRAPHENE

#### A. Basic definitions

Let us consider that a carbon atom on the otherwise perfect lattice of graphene has been replaced by a different type of atom. What will happen is a renormalization of both the on-site energy, and the hopping parameter between that atom and the nearest-neighbor carbon atoms. If the hopping parameter of clean graphene is  $t$  then the hopping between the impurity atom and the carbon atoms can be parametrized by an additional constant denoted  $t_0$ , as shown in Fig. 1. The value of  $t_0$  can be varied: if the impurity atom is strongly coupled to the carbon atom,  $t_0$  will be negative; if, on the other hand, the coupling is weak,  $t_0$  will be positive. The Hamiltonian of the system will be that of clean graphene and a term representing the renormalization of the hopping, as explained below.<sup>35</sup>

Let us first introduce some definitions for latter use. The honeycomb lattice has a unit cell represented in Fig. 1 by the vectors  $\mathbf{a}_1$  and  $\mathbf{a}_2$ , such that  $|\mathbf{a}_1|=|\mathbf{a}_2|=a$ , with  $a \approx 2.461 \text{ \AA}$ . In this basis any lattice vector  $\mathbf{R}$  is represented as

$$\mathbf{R} = n\mathbf{a}_1 + m\mathbf{a}_2, \quad (1)$$

with  $n, m$  integers. In Cartesian coordinates one has

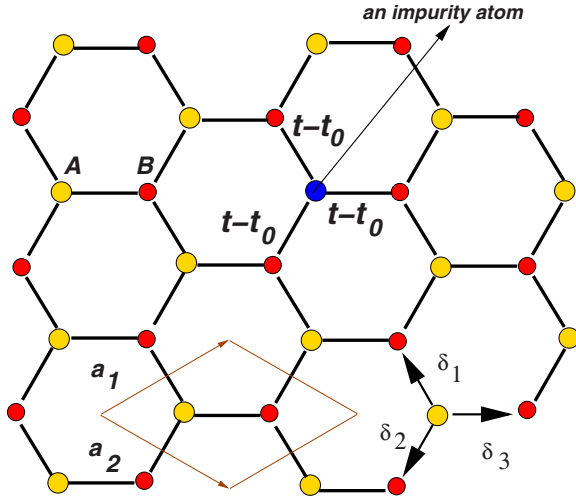


FIG. 1. (Color online) The honeycomb lattice with a substituting atom replacing a carbon atom. The local hopping parameter changes from  $t$  to  $t-t_0$  around the A atom. We assume all over  $t = 3$  eV.

$$\mathbf{a}_1 = \frac{a_0}{2}(3, \sqrt{3}, 0), \quad \mathbf{a}_2 = \frac{a_0}{2}(3, -\sqrt{3}, 0), \quad (2)$$

where  $a_0 = a/\sqrt{3}$  is the carbon-carbon distance.

If periodic boundary conditions are used, the Bloch states are characterized by momentum vectors of the form

$$\mathbf{k} = \frac{m_1}{N_1}\mathbf{b}_1 + \frac{m_2}{N_2}\mathbf{b}_2, \quad (3)$$

with  $m_1$  and  $m_2$  as a set of integers running from 0 to  $N_1 - 1$  and from 0 to  $N_2 - 1$ , respectively. The numbers  $N_1$  and  $N_2$  are the number of unit cells along the  $\mathbf{a}_1$  and  $\mathbf{a}_2$  directions, respectively. The total number of unit cells is, therefore,  $N_c = N_1 N_2$ . The reciprocal-lattice vectors are given by

$$\mathbf{b}_1 = \frac{2\pi}{3a_0}(1, \sqrt{3}, 0), \quad \mathbf{b}_2 = \frac{2\pi}{3a_0}(1, -\sqrt{3}, 0). \quad (4)$$

The vectors connecting any A atom to its nearest neighbors read

$$\delta_1 = \frac{a_0}{2}(-1, \sqrt{3}, 0) = \frac{1}{3}(\mathbf{a}_1 - 2\mathbf{a}_2), \quad (5)$$

$$\delta_2 = \frac{a_0}{2}(-1, -\sqrt{3}, 0) = \frac{1}{3}(\mathbf{a}_2 - 2\mathbf{a}_1), \quad (6)$$

$$\delta_3 = a_0(1, 0, 0) = \frac{1}{3}(\mathbf{a}_1 + \mathbf{a}_2). \quad (7)$$

Using the above definitions the Hamiltonian for this problem can be written as

$$H_0 = -t \sum_{\mathbf{R}} [a(\mathbf{R})b^\dagger(\mathbf{R}) + a(\mathbf{R})b^\dagger(\mathbf{R} - \mathbf{a}_2) + a(\mathbf{R})b^\dagger(\mathbf{R} - \mathbf{a}_1) + \text{H.c.}], \quad (8)$$

which represents clean graphene (the spin index is omitted

for simplicity of writing), and the perturbation due to the impurity atom is

$$V_i = t_0[a(0)b^\dagger(0) + a(0)b^\dagger(-\mathbf{a}_2) + a(0)b^\dagger(-\mathbf{a}_1) + \text{H.c.}]. \quad (9)$$

It is assumed that the impurity atom is in the unit cell  $\mathbf{R} = 0$  but there is no loss of generalization due to this choice. In the particular case of  $t_0 = t$ , the scattering term  $V_i$  represents a vacancy since the impurity atom is completely decoupled from the carbon atoms. It is important to keep in mind that in a given unit cell both A and B types of atoms are described by the same vector  $\mathbf{R}$ .

The calculation of the electronic properties of graphene requires the calculation of the corresponding Green's functions, whose definitions are

$$G_{aa}(\mathbf{k}, \mathbf{q}, \tau) = -\langle T[a_{\mathbf{k}}(\tau)a_{\mathbf{q}}^\dagger(0)] \rangle, \quad (10)$$

$$G_{bb}(\mathbf{k}, \mathbf{q}, \tau) = -\langle T[b_{\mathbf{k}}(\tau)b_{\mathbf{q}}^\dagger(0)] \rangle, \quad (11)$$

$$G_{ab}(\mathbf{k}, \mathbf{q}, \tau) = -\langle T[a_{\mathbf{k}}(\tau)b_{\mathbf{q}}^\dagger(0)] \rangle, \quad (12)$$

$$G_{ba}(\mathbf{k}, \mathbf{q}, \tau) = -\langle T[b_{\mathbf{k}}(\tau)a_{\mathbf{q}}^\dagger(0)] \rangle, \quad (13)$$

and their Fourier transform to the Matsubara representation are given in Appendix for the case of a perfect lattice. Of particular interest to our calculations is the momentum integral of the retarded diagonal Green's function

$$\bar{G}_{AA}^0(\omega) = \frac{1}{N_c} \sum_{\mathbf{k}} G_{AA}^0(\mathbf{k}, \omega). \quad (14)$$

The integral is best performed using the density of states of the honeycomb lattice. Since we want to take into account the nonlinearity of the bands, which allows us to describe the properties of the system at large energies and not only those close to the Dirac point, we have to use for the density of states an expression that goes beyond the usually used linear dependence of this quantity on energy. In a previous work<sup>36</sup> we derived an expansion for the density of states (per unit cell, per spin) valid for energies up to  $\sim 3$  eV, reading ( $E = \hbar\omega$ )

$$\rho(E) \simeq \frac{2E}{\sqrt{3}\pi t^2} + \frac{2E^3}{3\sqrt{3}\pi t^4} + \frac{10E^5}{27\sqrt{3}\pi t^6}. \quad (15)$$

The imaginary part of  $\bar{G}_{AA}^0(\omega)$  reads

$$\Im \bar{G}_{AA}^0(\omega) = -\frac{\pi}{2}\rho(\hbar\omega), \quad (16)$$

and the real part has the form

$$\Re \bar{G}_{AA}^0(\omega) = P_1(\hbar\omega) + P_2(\hbar\omega) \ln \frac{(\hbar\omega)^2}{D_c^2 - (\hbar\omega)^2}, \quad (17)$$

where  $P_1(x)$  and  $P_2(x)$  are polynomial functions given by

$$P_1(x) = -\frac{x}{3t^2} - \frac{5}{27t^4} \left( \frac{x}{2} D_c^2 + x^3 \right), \quad (18)$$

$$P_2(x) = \frac{x}{D_c^2} + \frac{x^3}{3t^2 D_c^2} + \frac{5}{27D_c^2 t^4} x^5. \quad (19)$$

The energy  $D_c$  is a cutoff energy chosen as  $D_c^2 = \sqrt{3} \pi t^2$ .

### B. Exact Green's Functions

We now want to determine the exact expressions for the Green's functions in the presence of the substituting atom. This is best accomplished using the equation of motion method. The equations of motion for the Green's functions can be readily established, and read as

$$i\omega_n G_{AA}(\omega_n, \mathbf{k}, \mathbf{p}) = \delta_{\mathbf{k}, \mathbf{p}} + t\phi(\mathbf{k})G_{BA}(\omega_n, \mathbf{k}, \mathbf{p}) - \frac{t_0}{N_c} \sum_{\mathbf{k}'} \phi(\mathbf{k}')G_{BA}(\omega_n, \mathbf{k}', \mathbf{p}), \quad (20)$$

$$i\omega_n G_{BA}(\omega_n, \mathbf{k}, \mathbf{p}) = t\phi^*(\mathbf{k})G_{AA}(\omega_n, \mathbf{k}, \mathbf{p}) - \frac{t_0}{N_c} \phi^*(\mathbf{k}) \sum_{\mathbf{k}'} G_{AA}(\omega_n, \mathbf{k}', \mathbf{p}), \quad (21)$$

$$i\omega_n G_{AB}(\omega_n, \mathbf{k}, \mathbf{p}) = t\phi(\mathbf{k})G_{BB}(\omega_n, \mathbf{k}, \mathbf{p}) - \frac{t_0}{N_c} \sum_{\mathbf{k}'} \phi(\mathbf{k}')G_{BB}(\omega_n, \mathbf{k}', \mathbf{p}), \quad (22)$$

$$i\omega_n G_{BB}(\omega_n, \mathbf{k}, \mathbf{p}) = \delta_{\mathbf{k}, \mathbf{p}} + t\phi^*(\mathbf{k})G_{AB}(\omega_n, \mathbf{k}, \mathbf{p}) - \frac{t_0}{N_c} \phi^*(\mathbf{k}) \sum_{\mathbf{k}'} G_{AB}(\omega_n, \mathbf{k}', \mathbf{p}). \quad (23)$$

The complex number  $\phi(\mathbf{k})$  is defined as

$$\phi(\mathbf{k}) = 1 + e^{ik \cdot \mathbf{a}_1} + e^{ik \cdot \mathbf{a}_2} = 1 + e^{ik \cdot (\delta_3 - \delta_1)} + e^{ik \cdot (\delta_3 - \delta_2)}, \quad (24)$$

which is the form factor of the three  $B$  atoms as seen by an atom in  $A$ . The above set of equations can be solved exactly. The fact that the scattering term  $V_i$  depends on  $\phi(\mathbf{k})$  and that a single impurity breaks particle-hole symmetry of the system implies a complex form for  $T$  matrix. In fact, the general expression for the Green's functions does not have exactly the same form as in the case of one-band electrons. The solution of the equations of motion is rather lengthy and in the course of the solution we use the two following identities:

$$i\omega_n \sum_{\mathbf{k}} G_{AA}(\omega_n, \mathbf{k}, \mathbf{p}) = 1 + (t - t_0) \sum_{\mathbf{k}} \phi(\mathbf{k})G_{BA}(\omega_n, \mathbf{k}, \mathbf{p}), \quad (25)$$

and

$$t_0 z = -[(i\omega_n)^2 + z t_0(t - t_0)] \sum_{\mathbf{k}} \phi(\mathbf{k})G_{BA}(\omega_n, \mathbf{k}, \mathbf{p}) + i\omega_n t \sum_{\mathbf{k}} |\phi(\mathbf{k})|^2 G_{AA}(\omega_n, \mathbf{k}, \mathbf{p}), \quad (26)$$

with

$$z = \frac{1}{N_c} \sum_{\mathbf{k}} |\phi(\mathbf{k})|^2. \quad (27)$$

The use of relations (25) and (26) leads to

$$\sum_{\mathbf{k}} G_{AA}(\omega_n, \mathbf{k}, \mathbf{p}) = \frac{N_1(\mathbf{p}, \omega_n)}{D(\omega_n)}, \quad (28)$$

with the following definitions

$$N_1(\mathbf{p}, \omega_n) = (t - t_0)G_{AA}^0(\omega_n, \mathbf{p}) + t_0 \bar{G}_{AA}^0(\omega_n), \quad (29)$$

$$D(\omega_n) = (t - t_0)(1 - t_0/t) + i\omega_n(2t_0 - t_0^2/t) \bar{G}_{AA}^0(\omega_n), \quad (30)$$

$$\bar{G}_{AA}^0(\omega_n) = \frac{1}{N_c} \sum_{\mathbf{k}} G_{AA}^0(\omega_n, \mathbf{k}), \quad (31)$$

and

$$\tilde{G}_{AA}^0(\omega_n) = \frac{1}{N_c} \sum_{\mathbf{k}} |\phi(\mathbf{k})|^2 G_{AA}^0(\omega_n, \mathbf{k}). \quad (32)$$

The result [Eq. (28)] has the appropriate limiting behavior: when  $t_0 \rightarrow t$  one obtains  $(i\omega_n)^{-1}$ , which agrees with Eq. (25); when  $t_0 \rightarrow 0$  one obtains  $G_{AA}^0(\omega_n, \mathbf{p})$ , which is the result for the perfect lattice.

Finally, the exact solution for  $G_{AA}(\omega_n, \mathbf{k}, \mathbf{p})$ , considering an arbitrary value of  $t_0$ , has the following structure

$$G_{AA}(\omega_n, \mathbf{k}, \mathbf{p}) = \delta_{\mathbf{k}, \mathbf{p}} G_{AA}^0(\omega_n, \mathbf{k}) + G_{AA}^0(\omega_n, \mathbf{k}) \Sigma(\omega_n) + g(\omega_n) + G_{AA}^0(\omega_n, \mathbf{k}) T_{AA}(\mathbf{k}, \mathbf{p}, \omega_n) G_{AA}^0(\omega_n, \mathbf{p}), \quad (33)$$

with

$$g(\omega_n) = \frac{1}{N_c} \frac{t_0^2 \bar{G}_{AA}^0(\omega_n)}{t D(\omega_n)}, \quad (34)$$

$$\Sigma(\omega_n) = \frac{1}{N_c} \frac{t_0(1 - t_0/t)}{D(\omega_n)}, \quad (35)$$

and  $T_{AA}(\mathbf{k}, \mathbf{p}, \omega_n)$  given by

$$T_{AA}(\mathbf{k}, \mathbf{p}, \omega_n) = \frac{1}{N_c} \frac{t(t_0 - t) |\phi(\mathbf{k})|^2 - (i\omega_n)^2}{t_0 i\omega_n D(\omega_n)}. \quad (36)$$

Clearly, solution (33) does not have the simple form of the  $T$  matrix as in the case of the solution of the scattering problem by a local potential in the single energy-band case. The calculation for  $G_{BB}(\omega_n, \mathbf{k}, \mathbf{p})$  proceeds along the same lines and gives

$$G_{BB}(\omega_n, \mathbf{k}, \mathbf{p}) = \delta_{\mathbf{k}, \mathbf{p}} G_{BB}^0(\omega_n, \mathbf{k}) + G_{BB}^0(\omega_n, \mathbf{k}) T_{BB}(\mathbf{k}, \mathbf{p}, \omega_n) G_{BB}^0(\omega_n, \mathbf{p}), \quad (37)$$

with  $T_{BB}(\mathbf{k}, \mathbf{p}, \omega_n)$  given by

$$T_{BB}(\mathbf{k}, \mathbf{p}, \omega_n) = -\frac{1}{N_c} \frac{\phi^*(\mathbf{k})(2t - t_0)t_0\phi(\mathbf{p})}{i\omega_n D(\omega_n)}. \quad (38)$$

It is interesting to note that in the case of Eq. (37) the  $T$  matrix has the traditional form. So, as long as one does not

sit on top of the impurity atom, the scattering equations are similar to those of the scattering of the electron gas by a local potential. Exact results (33) and (37) are what are needed to discuss the behavior of current versus bias in STM experiments when the microscope tip comes near to a substituting defect.

### III. LOCAL DENSITY OF STATES

As we will see later, the properties of the STM current will depend on the local density of states below the tip of the microscope. We therefore have to compute this quantity for different circumstances. Because each unit cell is identified by a single vector  $\mathbf{R}$ , the local density of states (per spin) at the atoms  $A$  and  $B$  of the unit cell localized in the position  $\mathbf{R}$  is defined as

$$\rho_x(\mathbf{R}, \omega) = -\frac{1}{\pi N_c} \text{Im} G_{xx}(\mathbf{R}, \mathbf{R}, \omega), \quad (39)$$

with  $G_{xx}(\mathbf{R}, \mathbf{R}, \omega)$  ( $x=A, B$ ) obtained from

$$G_{xx}(\mathbf{R}, \mathbf{R}, \omega_n) = \sum_{\mathbf{k}, \mathbf{p}} e^{i(\mathbf{k}-\mathbf{p}) \cdot \mathbf{R}} G_{xx}(\mathbf{k}, \mathbf{p}, \omega_n), \quad (40)$$

after the usual analytical continuation  $\omega_n \rightarrow \omega + i0^+$  of the Matsubara Green's function.

Let us first consider the case  $t_0 = t$ . With this choice the  $A$  atom is disconnected from the rest of the lattice and in this situation the momentum sum over the full  $G_{AA}(\omega_n, \mathbf{k}, \mathbf{p})$  reads

$$\sum_{\mathbf{k}} G_{AA}(\omega_n, \mathbf{k}, \mathbf{p}) = \frac{1}{i\omega_n}, \quad (41)$$

which corresponds to an isolated atom. As a consequence the local density of states is a delta function and no charge transport can take place through that atom. In the material this situation never happens and therefore we can interpret this result as the case where there is a vacancy in the lattice. Therefore the presence of a vacancy can be detected by its influence on the electronic density of states of the neighboring atoms (the  $B$  atom in the case of Fig. 1). Using only the first term in Eq. (15) it is possible to derive a relatively simple expression for the local density of states at the  $B$  atom near the vacancy, reading

$$\rho_B(0, \omega) = \frac{2}{\sqrt{3}\pi t} \left| \frac{\hbar\omega}{t} \right| \left( \left| 1 - \frac{1}{9} \left| \frac{\hbar\omega}{t} \right|^2 + \frac{1}{3} \left| \frac{t}{\hbar\omega} \right|^2 \right|^2 L(\omega) \right), \quad (42)$$

with

$$L(\omega) = \left[ 1 + \frac{1}{\pi^2} \ln^2 \left( \frac{1}{\sqrt{3}\pi} \left| \frac{\hbar\omega}{t} \right|^2 \right) \right]^{-1}. \quad (43)$$

It is also possible to determine general analytical expressions for  $\rho_A(0, \omega)$  and  $\rho_B(0, \omega)$ , given an arbitrary value of  $t_0$ , but due to the form of  $D(i\omega_n)$ , which in this case depends on both  $t$  and  $t_0$ , the final result is somewhat cumbersome. However, if really needed, it is straightforward to use the full

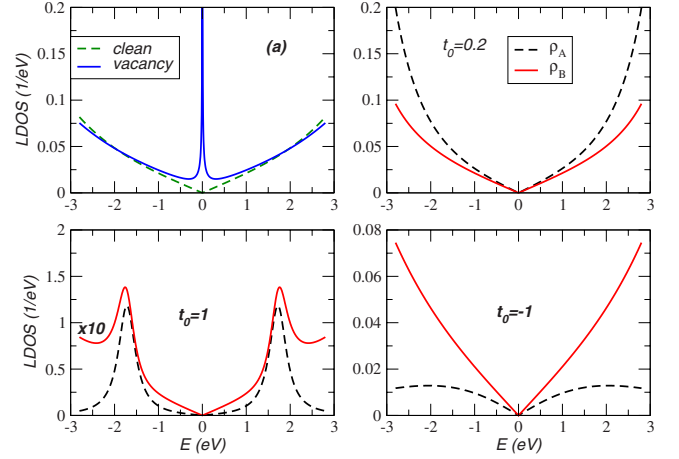


FIG. 2. (Color online) Local density of states (LDOS) at the unit cell  $\mathbf{R}=0$  for the  $A$  and  $B$  atoms, and different values of  $t_0$  in electron volt. In panel (a) we plot the density of states of clean graphene and the LDOS at the  $B$  atom near a vacancy at the  $A$  atom of the same unit cell. For  $t_0=1$ ,  $\rho_B(0, \omega)$  is multiplied by ten for clarity.

equations for  $G_{AA}$  and  $G_{BB}$ , and the given expressions for  $\bar{G}_{AA}(\omega)$  to write down analytical expression for the density of states.

In Fig. 2 we plot the local density of states for different values of  $t_0$ . In panel (a) of that figure we represent the density of states at a  $B$  site in the unit cell where a vacancy exists in the  $A$  atom of the same unit cell. The most significant feature is a development of a logarithmic divergence at zero energy. Therefore the clean density of states (also shown for comparison) is strongly modified by the presence of such a strong potential. For a moderate value of  $t_0$  the change in the hopping is not strong, and the density of states at both the  $A$  and  $B$  atoms retain the linearity of the clean density of states close to the Dirac point. However, the absolute value of the two density of states are not the same and a clear deviation from linearity is seen to take place for lower energies when compared with the clean case. If the impurity atom binds strongly to the carbon atoms ( $t_0=-1$ ), there is an increase in the density of states at the neighbor atoms at the expenses of the density of states of the impurity. On the other hand, if the impurity binds weakly to the carbon atoms ( $t_0=1$ ), the density of states increases at the impurity and strong resonances develop on the impurity density of states. Clearly these different behaviors of the density of states will show up in the tunneling current.

It is also instructive to compute the local density of states as one moves away from the defect. This amounts to performing the Fourier transforms for finite  $\mathbf{R}$  in Eq. (40). In the case of  $G_{AA}(\mathbf{R}, \mathbf{R}, \omega)$  the calculation of the integrals is facilitated by the fact that the momentum space Green's function on the sublattice  $A$  depends on  $|\phi(\mathbf{k})|$  only, whereas in the case of the Green's function on the  $B$  sublattice this is not the case. Besides for finite  $\mathbf{R}$  the useful relation (A8) is valid no more. However, for large  $R=|\mathbf{R}|$  values when compared to  $a$ , i.e., away from the defect, the details of the lattice are no longer important, and the behavior of the local density of states at both the  $A$  and  $B$  sublattices must be similar, but out

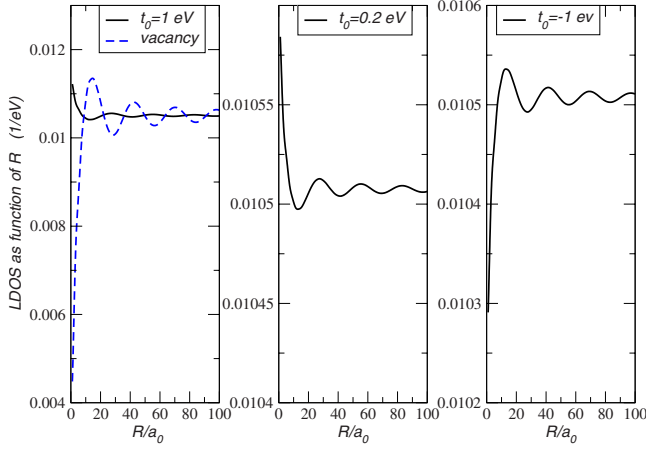


FIG. 3. (Color online) LDOS at distance  $R$  from unit cell  $\mathbf{R}=0$ , where the impurity is located for different values of  $t_0$ . The energy is  $\hbar\omega=0.5$  eV. The case of the vacancy is also illustrated.

of phase by  $\pi$ . We will therefore give the density of states as function of  $|\mathbf{R}|$  for the  $A$  sublattice only. Performing the Fourier transforms using the Dirac cone approximation (this is not a restriction and helps keeping the final result from becoming too cumbersome), one obtains (for the retarded function)

$$G_{xx}(\mathbf{R}, \mathbf{R}, \omega) = N_c \bar{G}_{AA}^0(\omega) + N_c \frac{A_c^2 \omega}{2\pi^2 v_F^2 D(\omega)} \Theta(\omega), \quad (44)$$

where  $v_F = 3a_0 t / (2\hbar)$  and  $\Theta(\omega)$  can be written as

$$\Theta(\omega) = t_0(t_0/t - 2) \frac{\omega^2}{2v_F^2} I^2(\omega), \quad (45)$$

where  $I(\omega)$  is defined as

$$I(\omega) = I_0(\omega) - i\pi \operatorname{sgn}(\omega) J_0(|\omega|R/v_F), \quad (46)$$

with  $J_0(x)$  as the Bessel function of integer order  $n=0$ , and finally  $I_0(\omega)$  is the Cauchy principal value of the integral

$$I_0(\omega) = \int_0^{k_c R} dx \frac{2x J_0(x)}{\alpha^2 - x^2}, \quad (47)$$

which can be evaluated using standard numerical methods. Moreover we also have  $k_c = 2\sqrt{\pi}/(\sqrt{3}\sqrt{3}a_0)$ , and  $\alpha = \omega R/v_F$ . In Fig. 3 we depict the local density of states at the carbon atoms located in the  $A$  sublattice, computed using Eq. (39). The typical oscillations in the density of states close to impurity centers are clearly seen. Note that as one moves away from the impurity the density of states approaches that of the clean system. The Friedel oscillations in graphene can be obtained from integrating the density of states up to the Fermi energy.

#### IV. CALCULATION OF THE TUNNELING CURRENT

We now want to compute the tunneling current between the tip of an STM microscope and graphene, when the tip is close to an impurity atom. We model the tip by a one-

dimensional tight-binding system, a standard approach.<sup>37,38</sup> Our results will not depend significantly from this choice as long as we assume a large value for the hopping parameter of the electrons in the tip. This choice essentially corresponds to represent the tip by a metal with a large bandwidth. Given the above, the Hamiltonian for the tip has the form

$$H = -V \sum_{n=-\infty}^{-1} [c^\dagger(n-1)c(n) + c(n)c^\dagger(n-1)] + H_0, \quad (48)$$

and  $H_0$  represents the Hamiltonian of the last atom of the tip. This choice corresponds to the assumption that the surface atom of the tip has a different nature from the atoms in the bulk of tip. We therefore represent  $H_0$  by

$$H_0 = \epsilon_0 c^\dagger(0)c(0) - W_1 [c^\dagger(-1)c(0) + c(0)c^\dagger(-1)]. \quad (49)$$

It is essential that the Hamiltonian of the tip be represented by a semi-infinite metal since otherwise there would be electrons reflected at the far end of the tip modifying in this way the tunneling current. Finally we need to include the tunneling of the electrons of the tip to graphene. There are a number of ways we can do this. Here we assume that the coupling is made directly either to the impurity atom or to the next neighbor carbon atom. This choice corresponds to probing the local electronic properties at or around the impurity. More general types of coupling are easily included in the formalism. We write this coupling as

$$H_T = -W_2 [c^\dagger(0)d(0) + d^\dagger(0)c(0)], \quad (50)$$

where the operator  $d(0)$  can represent either the impurity atom at the  $A$  sublattice or the carbon atom at the  $B$  sublattice.

Since the Hamiltonian of the problem is bilinear we can write it in matrix form (of infinite dimension) as

$$H = \begin{bmatrix} H_b & V_L & 0 \\ V_L^\dagger & H_0 & V_R^\dagger \\ 0 & V_R & H_g \end{bmatrix}, \quad (51)$$

where the matrices  $V_L$  and  $V_R$  represent the coupling of the last atom in the tip of the STM microscope to the bulk of the tip and to graphene, respectively, and  $H_b$  and  $H_g$  stand for the bulk Hamiltonians of the tip and of graphene, including impurity potential (9), respectively.

The tunneling is a local property, controlled by the coupling of the last atom of the tip to the bulk atoms and to graphene. Since we want to compute local quantities, this is best accomplished using Green's functions in real space. The full Green's function of the system is defined by

$$(1E + i0^+ - H)G^+ = 1, \quad (52)$$

where we have chosen the retarded function (denoted with the  $+$  superscript), and  $1$  is the identity matrix. The matrix form of the Green's function is

$$G^+ = \begin{bmatrix} G_{bb} & G_{b0} & G_{bg} \\ G_{0b} & G_{00} & G_{0g} \\ G_{gb} & G_{g0} & G_{gg} \end{bmatrix}. \quad (53)$$

The quantity of interest is  $G_{00}$ , which can be shown to have the form

$$G_{00}^+ = (E + i0^+ - \epsilon_0 - \Sigma_L^+ - \Sigma_R^+), \quad (54)$$

where the matrices  $\Sigma_L^+$  and  $\Sigma_R^+$  are the self-energies and have the form

$$\Sigma_L^+ = W_1^2 G_s^+, \Sigma_R^+ = W_2^2 G_{xx}^+, \quad (55)$$

where the Green's functions  $G_s^+$  and  $G_{xx}^+$  are the surface Green's function of the Hamiltonians  $H_b$  and  $H_g$  at the impurity unit cell ( $x=A, B$ ), respectively. Note that the quantity  $G_{xx}^+$  is computed using Eq. (44) making  $\mathbf{R}=0$ . It is possible to find a close form for  $G_{xx}^+$ , as we have shown in the previous section. Also for  $G_s^+$  a close form exists<sup>39-41</sup>

$$G_s^+ = [E + i0^+ - V^2 G_s^+]^{-1}. \quad (56)$$

The solution of Eq. (56) is elementary and reads

$$G_s^+ = \frac{E}{2V^2} - \frac{i}{2V^2} \sqrt{4V^2 - E^2}, \quad (57)$$

for  $E^2 < 4V^2$  and

$$G_s^+ = \frac{E}{2V^2} - \frac{\text{sgn}(E)}{2V^2} \sqrt{E^2 - 4V^2}, \quad (58)$$

for  $E^2 > 4V^2$ .

Our goal is to study the STM current at finite bias, which is a particular case of nonequilibrium transport. This is done using the nonequilibrium Green's function method or Keldysh method. This method is particularly suited to study the regime where the system has a strong departure from equilibrium, such as when the bias potential  $V_b$  is large. We consider that, however, the system is in the steady state. Since the seminal paper of Caroli *et al.*<sup>42</sup> on nonequilibrium quantum transport, the method of nonequilibrium Green's functions started to be generalized to the calculation of transport quantities of nanostructures. There are many places where one can find a description of the method<sup>43,44</sup> but a recent and elegant one was introduced in the context of transport through systems that have bound states, showing that the problem can be reduced to the solution of a kind of quantum Langevin equation.<sup>45</sup>

The general idea in this method is that two perfect leads are coupled to our system, which is usually called the device. In our case the device is defined by the last atom at the tip of the microscope. The Green's function of the device has to be computed in the presence of the bulk of the tip and of graphene. This corresponds to our  $G_{00}^+$  Green's function. Besides the Green's function we need the effective coupling between the last atom of the tip and the bulk atoms as well as the coupling to the graphene atoms, which are determined in terms of the self-energies

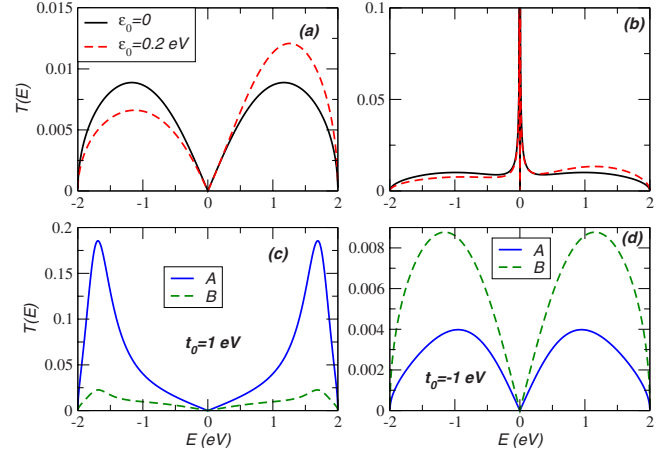


FIG. 4. (Color online) Transmission coefficient  $T(E)$  as function of the energy for zero bias. The fixed parameters are  $t=3.0$ ,  $V=1$ ,  $W_1=0.9$ , and  $W_2=0.2$ , all in electron volt. Panel (a) depicts the case of clean graphene and two different values of  $\epsilon_0$ . Panel (b) depicts  $T(E)$  through a  $B$  site when a vacancy sits at the  $A$  site. Panel (c) depicts  $T(E)$  through  $A$  and  $B$  sites, when an impurity sits at the  $A$  site, taking  $t_0=1$  eV and  $\epsilon_0=0$ . Panel (d) is the same as panel (c) for  $t_0=-1$  eV.

$$\Gamma_{L/R} = \frac{i}{2\pi} (\Sigma_{L/R}^+ - \Sigma_{L/R}^-). \quad (59)$$

Therefore the effective coupling  $\Gamma_{L/R}$  depends on the surface Green's function of the tip and of graphene. According to the general theory, the two systems (bulk of the tip and graphene) are in thermal equilibrium at temperatures  $T_{L/R}$  and chemical potential  $\mu_{L/R}$ , and are connected to the system at some time  $t_0$ . The bottom line is that the total current through the device is given by (both spins included)

$$J = \frac{2e}{h} \int_{-\infty}^{\infty} dE T(E) [f(E, \mu_L, T_L) - f(E, \mu_R, T_R)], \quad (60)$$

where  $f(x)$  is the Fermi-Dirac distribution and the transmission  $T(E)$  is given by

$$T(E) = 4\pi^2 \text{Tr}[\Gamma_L G_{00}^+ \Gamma_R G_{00}^-]. \quad (61)$$

Performing the trace (which in this case is only a product of complex numbers) we obtain

$$T(E) = 4W_1^2 W_2^2 \Im G_s^+ \Im G_{xx}^+ |G_{00}^+|^2. \quad (62)$$

Figure 4 represents  $T(E)$  in several conditions. In the clean case, we see the effect the Dirac point has on the transmission, leading to a suppression of the tunneling for  $E \approx 0$ . It is also clear that the parameters characterizing the last atom of the tip strongly influences the form of  $T(E)$ , leading to an asymmetry between negative and positive energies due to the finiteness of  $\epsilon_0$ . When a vacancy is present at the  $A$  site, the tunneling through the nearest  $B$  sites is strongly modified relatively to the clean case, with strong tunneling taking place at energies very close to the Dirac point. When an impurity atom sits at the  $A$  site the behavior of the tunneling probability depends on the coupling between the impurity and the carbon atoms. In the case of weak coupling to

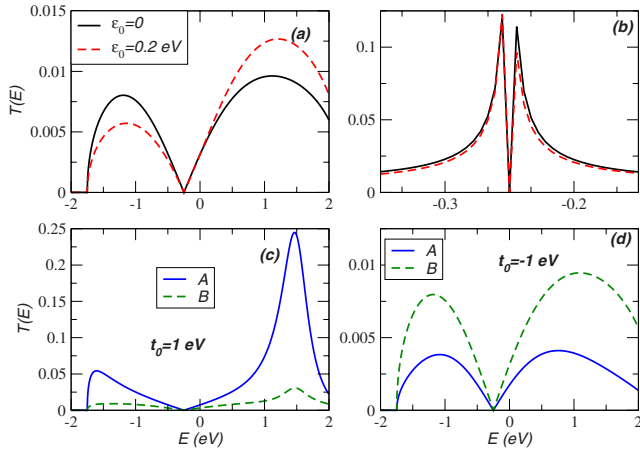


FIG. 5. (Color online) Transmission coefficient  $T(E)$  as function of the energy for finite bias  $V_b = 0.5$  V. The parameters and the description are the same as those listed in the caption of Fig. 4. The energy scale in the case of the vacancy was increased in order to see the low-energy behavior close to the Dirac point.

the carbon atoms ( $t_0 > 0$ ), the tunneling through the *A* atom is facilitated relative to the tunneling between the nearest carbon atoms. When the impurity is strongly coupled to the carbon atoms ( $t_0 < 0$ ), the reverse happens. This behavior is easily understood since strong (weak) coupling to the carbon atoms is equivalent to a weak (strong) coupling to the tip of the microscope, leading to weaker (stronger) tunneling probability from the tip to graphene.

All the above discussion applies to zero-bias voltage. When finite bias voltage is applied between the tip and graphene, the behavior of the curves change. We will consider that the chemical potentials of the tip and of graphene differ by the electrostatic energy  $eV_b$ , where  $V_b$  is bias potential. This amounts to changing the on-site energies relative to their value in equilibrium. We choose to change the on-site energies of the tip by  $eV_b/2$  and those of the carbon atoms by  $-eV_b/2$ . In Fig. 5 we depict  $T(E)$  for a finite value of the bias  $V_b$ . The most distinctive difference relative to the case of zero bias is the energy asymmetry induced by the bias relatively to the case of zero bias, even when  $\epsilon_0 = 0$ .

The calculation of the current also depends on the chemical potential. In the case of graphene this can be tuned by a back gate  $V_g$ . The relation between the back gate voltage and the chemical potential of graphene obeys the relation

$$\mu = v_F \hbar \sqrt{\frac{\pi \epsilon \epsilon_0 V_g}{de}}, \quad (63)$$

which is numerically equal to  $\mu = 0.03 \sqrt{V_g}$  in electron volt. The parameters in Eq. (63) are  $\epsilon = 3.9$ , the dielectric constant of  $\text{SiO}_2$ ,  $d = 300$  nm, the thickness of the  $\text{SiO}_2$  substrate, and  $e$  is the elementary charge. Taking a typical value of  $V_g = 100$  V we obtain  $\mu = 0.3$  eV, which is the value we assume for the chemical potential in the calculations below. Since we will perform our calculations at zero temperature, the current is given by

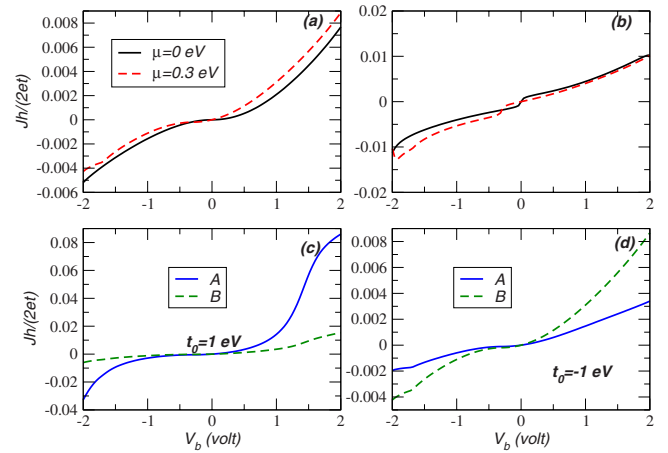


FIG. 6. (Color online) Current  $J$  as function of the bias voltage  $V_b$ . The parameters are the same as those listed in the caption of Fig. 4 and  $\epsilon_0 = 0.2$  eV. Panel (a) represents the clean case for two values of the chemical potential  $\mu$ . The case of the vacancy is represented in panel (b), also for two values of the chemical potential. Panel (c) represents the case  $t_0 = 1$  eV for  $\mu = 0.3$  eV, and panel (d) is the same as (c) for  $t_0 = -1$  eV. In panels (c) and (d), *A* and *B* refer to tunneling through the atom sitings on sublattice *A* or *B*, respectively.

$$J = \frac{2e}{h} \int_{\mu - eV_b/2}^{\mu + eV_b/2} dE T(E, V_b). \quad (64)$$

The results for the calculation of  $J$  versus  $V_b$  is depicted in Fig. 6. Looking at them, we see that there is an asymmetry between the negative and positive values of  $V_b$ . For the clean case, it is clear that the magnitude of the  $J$  current does not depend much on the chemical potential, and therefore on the gate voltage  $V_g$ . The same is true for the vacancy case. Comparing the curves for the vacancy and for the clean case, we see that the order of magnitude of the current is the same but the shape of the curves is notoriously different from that of the clean case. When the impurity is weakly coupled ( $t_0 > 0$ ) to the carbon atoms, the tunneling current is facilitated through the impurity atom, as can be seen from panel (c) of Fig. 6, with an absolute value five times larger for  $V_b = 1$  volt. Also a clear jump is seen in  $J$  [panel (c)], a fingerprint of the resonances in the density of states is seen in panel (c) of Fig. 3. One notes that in Fig. 3 the resonances are symmetrically positioned relatively to the Dirac point but this is not so for the jumps in the current. The reason is due to finite on-site energy at the atom in the tip of the microscope. On the other hand for strong coupling [panel (d) of Fig. 6], there is not much difference from the clean case, apart from the fact that tunneling current through the impurity or the neighbor carbon atom has different magnitude.

Another important quantity to fully characterize the STM current is the shot noise.<sup>46</sup> For interacting systems this quantity gives information on the possible existence of quasiparticles with fractional charge. On disordered systems with no interactions, information on transport open channels can be obtained. For fermionic noninteracting electrons at zero temperature, the shot noise is defined as<sup>47</sup>

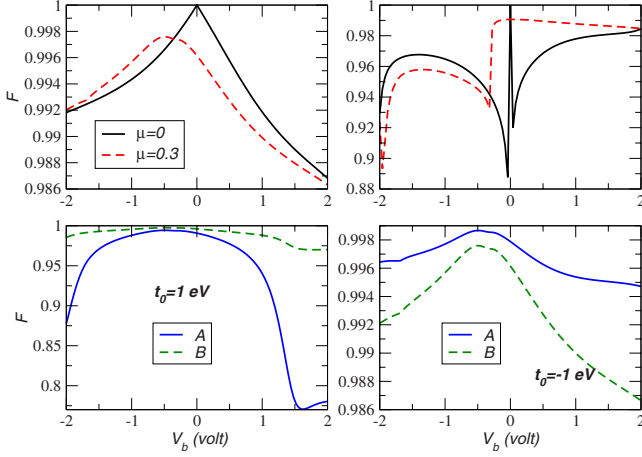


FIG. 7. (Color online) Fano factor  $F$  as function of the bias voltage  $V_b$ . The parameters are the same as those listed in the caption of Fig. 4 and  $\epsilon_0=0.2$  eV. Panel (a) represents the clean case for two values of the chemical potential  $\mu=0$  and  $\mu=0.3$  eV. The case of the vacancy is represented in panel (b), also for two values of the chemical potential. Panel (c) represents the case  $t_0=1$  eV for  $\mu=0.3$  eV, and panel (d) is the same as (c) for  $t_0=-1$  eV. In panels (c) and (d), A and B refer to tunneling through the atom sitings on sublattice A or B, respectively.

$$S = \frac{2e^2}{\hbar} \int_{\mu_R}^{\mu_L} dE T(E) [1 - T(E)]. \quad (65)$$

The relevant quantity is not  $S$  directly but the Fano factor<sup>46</sup> defined as

$$F = \frac{S}{eJ}. \quad (66)$$

When the transmission  $T(E)$  is strongly reduced we have  $F \rightarrow 1$ , and noise is said to be Poissonian. On the other hand, if the system has a finite density of open channels,  $T(E) \rightarrow 1$ , we have  $F < 1$  due to  $[1 - T(E)] \ll 1$ . In Fig. 7 we plot the Fano factor as function of the bias voltage.

Clearly, for all cases but the vacancy, the Fano factor is close to the Poissonian values  $F=1$ . When  $V_b \rightarrow 0$  and the chemical potential is zero, the value of  $T(E)$  is quite small due to the presence of the Dirac point, and the Fano factor takes the limiting value  $F=1$ . For the vacancy, we obtain much smaller values of  $F$ , which is an indication of the presence of the strong resonance seen in the local density of states for this case, which leads to an increase in the transmission. It should be noted that in the cases of finite  $t_0$ , the concavity of the curves for  $F$  as function of  $V_b$  allows distinguishing of the case of weak coupling  $t_0 > 0$  from the case of strong coupling  $t_0 < 0$ .

## V. DISCUSSION AND CONCLUSIONS

We have studied in detail the electronic local density of states in graphene close to a substituting atom. This quantity turns out to be important in STM experiments since the tunneling of the electrons from tip of the microscope to the sample is determined by this quantity. The shape and mag-

nitude of the tunneling current depends on the nature of the substituting atom. In the case of the vacancy the shape of the tunneling current has a very different signature from the other cases. Also the magnitude of the current depends on the strength of the bonding between the impurity and the carbon atom.

The curves we have presented here are only indicative of the general behavior of the density of states and of the tunneling current. In order to obtain experimentally relevant curves we should have real numbers for the parameters of the tip, with special importance for the last atom of tip. Also the parameter  $W_2$  could be modeled more accurately by introducing the spatial dependence between the tip and the graphene surface. Density-functional calculations can be used to model the tip in realistic way.

In our analysis we have considered that the electrons can only tunnel from the tip to the atom underneath but when the tip is between two atoms the tunnel will take place to more than one atom. However, in this case the amplitude  $W_2$  is strongly reduced and the tunneling current will show a minimum. In fact it can be shown that the self-energy has in this case the form

$$\Sigma_R^+ = \tilde{W}_2^2 (G_{AA}^+ + G_{BB}^+), \quad (67)$$

assuming that the tip is exactly in between the A and B atoms, and therefore the value of the current will be controlled mainly by the value of  $\tilde{W}_2$ .

As we have seen in the calculation of the density of states, the case of weak coupling leads to the appearance of resonances at large energy values. The scan of the bias in our calculations did not reach these energies but if it does a clear signature will be seen in the tunneling current. Also, for fixed bias, moving the tip away from the impurity will show oscillations in the STM current.

One ingredient not included in our model is the effect of on-site energies at the impurities.<sup>48</sup> As a consequence, a natural question is whether our results are strongly modified if this effect is included. One should note that the values of the on-site energy and the hopping are correlated with each other in the case of boron and nitrogen impurities. When the hopping is enhanced the on-site energy is positive relatively to that of the carbon atoms. In this case, the results of our calculations in the present work show no qualitative changes from the more general model, as more detailed calculations show. In the case of reduced hopping, the same resonances we see in the local density of states of our work are also present in the more general approach but their position in energy changes and an asymmetry of those resonances relatively to the Dirac point develops. One should also note that the different chemical nature of the atoms making the tip of the microscope also induces an asymmetry in the current even when the LDOS does not show such asymmetry. Therefore, a careful study is needed to disentangle the effects from the tip and from a finite on-site energy at the impurity atoms.

Another relevant question is whether the resonances seen in the density of states will broaden so much when the concentration of impurities increases leaving no trace of them in the LDOS. Our calculations naturally refer to the diluted



limit, where the distance between impurities is large. When the concentration increases the resonances will broaden but their fingerprints still remains in the LDOS.<sup>49</sup> In Ref. 49, Fig. 13(a) shows that the resonances remain well defined even for concentration of impurities up to 10%. It is not possible to give a characteristic length at the Dirac point such that above it the impurities could be considered acting isolated. This is so because Fermi momentum is zero. One should therefore rely on numerical calculations with a varying concentration of impurities as in Ref. 49.

### ACKNOWLEDGMENTS

This work was supported by FCT under the Grant No. PTDC/FIS/64404/2006. J. M. B. Lopes dos Santos is acknowledged for fruitful discussions.

### APPENDIX: FREE PROPAGATORS AND USEFUL RELATIONS

The propagators for the perfect lattice are ( $\hbar=1$ )

$$G_{AA}^0(\omega_n, \mathbf{k}, \mathbf{p}) = \frac{i\omega_n \delta_{\mathbf{k}, \mathbf{p}}}{(i\omega_n)^2 - t^2 |\phi(\mathbf{k})|^2}, \quad (\text{A1})$$

$$G_{BA}^0(\omega_n, \mathbf{k}, \mathbf{p}) = \frac{\delta_{\mathbf{k}, \mathbf{p}} \phi^*(\mathbf{k})}{(i\omega_n)^2 - t^2 |\phi(\mathbf{k})|^2}, \quad (\text{A2})$$

$$G_{BB}^0(\omega_n, \mathbf{k}, \mathbf{p}) = \frac{i\omega_n \delta_{\mathbf{k}, \mathbf{p}}}{(i\omega_n)^2 - t^2 |\phi(\mathbf{k})|^2}, \quad (\text{A3})$$

$$G_{AB}^0(\omega_n, \mathbf{k}, \mathbf{p}) = \frac{\delta_{\mathbf{k}, \mathbf{p}} \phi(\mathbf{k})}{(i\omega_n)^2 - t^2 |\phi(\mathbf{k})|^2}. \quad (\text{A4})$$

From these, integrals (31) and (32) are defined as

$$\bar{G}_{AA}^0(\omega_n) = i\omega_n \int \frac{\rho(E) dE}{(i\omega_n)^2 - E^2}, \quad (\text{A5})$$

$$\tilde{G}_{AA}^0(\omega_n) = \frac{i\omega_n}{t^2} \int \frac{E^2 \rho(E) dE}{(i\omega_n)^2 - E^2} = -i\omega_n t^{-2} + (i\omega_n)^2 t^{-2} \bar{G}_{AA}^0(\omega_n), \quad (\text{A6})$$

and

$$\rho(E) = \frac{A_c}{4\pi^2} \int_{\text{BZ}} d^2\mathbf{k} \delta(E - t|\phi(\mathbf{k})|), \quad (\text{A7})$$

where  $A_c = 3\sqrt{3}a_0/2$  is the area of the unit cell. With the above definition  $\rho(E)$  is finite in the energy range  $0 < E < 3t$ . In addition we also have the useful relation

$$\sum_{\mathbf{k}} \phi(\mathbf{k}) G_{AA}^0(\omega_n, \mathbf{k}) = \sum_{\mathbf{k}} \phi^*(\mathbf{k}) G_{AA}^0(\omega_n, \mathbf{k}) = \frac{N_c}{3} \tilde{G}_{AA}^0(\omega_n). \quad (\text{A8})$$

Similar equations hold for  $G_{BB}^0$ .

- 
- <sup>1</sup>K. S. Novoselov, A. K. Geim, S. V. Morozov, D. Jiang, Y. Zhang, S. V. Dubonos, I. V. Grigorieva, and A. A. Firsov, *Science* **306**, 666 (2004).
- <sup>2</sup>K. S. Novoselov, D. Jiang, T. Booth, V. V. Khotkevich, S. M. Morozov, and A. K. Geim, *Proc. Natl. Acad. Sci. U.S.A.* **102**, 10451 (2005).
- <sup>3</sup>A. H. Castro Neto, F. Guinea, N. M. R. Peres, K. S. Novoselov, and A. K. Geim, *Rev. Mod. Phys.* **81**, 109 (2009).
- <sup>4</sup>N. M. R. Peres, F. Guinea, and A. H. Castro Neto, *Phys. Rev. B* **73**, 125411 (2006).
- <sup>5</sup>V. M. Pereira, F. Guinea, J. M. B. Lopes dos Santos, N. M. R. Peres, and A. H. Castro Neto, *Phys. Rev. Lett.* **96**, 036801 (2006).
- <sup>6</sup>Y. V. Skrypnik and V. M. Loktev, *Phys. Rev. B* **73**, 241402(R) (2006).
- <sup>7</sup>V. V. Cheianov and V. I. Falko, *Phys. Rev. Lett.* **97**, 226801 (2006).
- <sup>8</sup>C. Bena, *Phys. Rev. Lett.* **100**, 076601 (2008).
- <sup>9</sup>M. A. H. Vozmediano, M. P. López-Sancho, T. Stauber, and F. Guinea, *Phys. Rev. B* **72**, 155121 (2005).
- <sup>10</sup>A. Cortijo and M. A. H. Vozmediano, *Nucl. Phys. B* **763**, 293 (2007).
- <sup>11</sup>O. V. Yazyev, I. Tavernelli, U. Rothlisberger, and L. Helm, *Phys. Rev. B* **75**, 115418 (2007).
- <sup>12</sup>O. V. Yazyev and L. Helm, *Phys. Rev. B* **75**, 125408 (2007).
- <sup>13</sup>N. M. R. Peres, A. H. Castro Neto, and F. Guinea, *Phys. Rev. B* **73**, 195411 (2006).
- <sup>14</sup>E. R. Mucciolo, A. H. Castro Neto, and C. H. Lewenkopf, *Phys. Rev. B* **79**, 075407 (2009).
- <sup>15</sup>E. Stolyarova, K. T. Rim, S. Ryu, J. Maultzsch, P. Kim, L. E. Brus, T. F. Heinz, M. S. Hybertsen, and G. W. Flynn, *Proc. Natl. Acad. Sci. U.S.A.* **104**, 9209 (2007).
- <sup>16</sup>M. I. Katsnelson and A. K. Geim, *Philos. Trans. R. Soc. London, Ser. A* **366**, 195 (2008).
- <sup>17</sup>A. Fasolino, J. H. Los, and M. I. Katsnelson, *Nature Mater.* **6**, 858 (2007).
- <sup>18</sup>J. Martin, N. Akerman, G. Ulbricht, T. Lohmann, J. H. Smet, K. von Klitzing, and A. Yacoby, *Nat. Phys.* **4**, 144 (2008).
- <sup>19</sup>D. C. Elias, R. R. Nair, T. M. G. Mohiuddin, S. V. Morozov, P. Blake, M. P. Halsall, A. C. Ferrari, D. W. Boukhvalov, M. I. Katsnelson, A. K. Geim, and K. S. Novoselov, *J. Am. Soc. Inf. Sci.* **323**, 610 (2009).
- <sup>20</sup>E. J. Mele and J. J. Ritsko, *Phys. Rev. B* **24**, 1000 (1981).
- <sup>21</sup>M. Endo, T. Hayashi, S.-H. Hong, T. Enoki, and M. S. Dresselhaus, *J. Appl. Phys.* **90**, 5670 (2001).
- <sup>22</sup>O. Stephan, P. M. Ajayan, C. Colliex, P. Redlich, J. M. Lambert, P. Bernier, and P. Lefin, *Science* **266**, 1683 (1994).
- <sup>23</sup>T. B. Martins, R. H. Miwa, A. J. R. da Silva, and A. Fazzio, *Phys. Rev. Lett.* **98**, 196803 (2007).
- <sup>24</sup>N. M. R. Peres, F. D. Klironomos, S.-W. Tsai, J. R. Santos, J. M. B. Lopes dos Santos, and A. H. Castro Neto, *Europhys. Lett.* **80**, 67007 (2007).

- <sup>25</sup>G. M. Rutter, J. N. Crain, N. P. Guisinger, T. Li, P. N. First, and J. A. Stroscio, *Science* **317**, 219 (2007).
- <sup>26</sup>P. Mallet, F. Varchon, C. Naud, L. Magaud, C. Berger, and J.-Y. Veuillen, *Phys. Rev. B* **76**, 041403(R) (2007).
- <sup>27</sup>V. W. Brar, Y. Zhang, Y. Yayon, T. Ohta, J. L. McChesney, A. Bostwick, E. Rotenberg, K. Horn, and M. F. Crommie, *Appl. Phys. Lett.* **91**, 122102 (2007).
- <sup>28</sup>M. Ishigami, J. H. Chen, W. G. Cullen, M. S. Fuhrer, and E. D. Williams, *Nano Lett.* **7**, 1643 (2007).
- <sup>29</sup>V. Geringer, M. Liebmann, T. Echtermeyer, S. Runte, M. Schmidt, R. Rckamp, M. Lemme, and M. Morgenstern, *Phys. Rev. Lett.* **102**, 076102 (2009).
- <sup>30</sup>Y. Zhang, V. W. Brar, F. Wang, C. Girit, Y. Yayon, M. Panlasigui, A. Zetl, and M. F. Crommie, *Nat. Phys.* **4**, 627 (2008).
- <sup>31</sup>A. Deshpande, W. Bao, F. Miao, C. N. Lau, and B. J. LeRoy, arXiv:0812.1073 (unpublished).
- <sup>32</sup>H. Amara, S. Latil, V. Meunier, Ph. Lambin, and J.-C. Charlier, *Phys. Rev. B* **76**, 115423 (2007).
- <sup>33</sup>T. O. Wehling, A. V. Balatsky, M. I. Katsnelson, A. I. Lichtenstein, K. Scharnberg, and R. Wiesendanger, *Phys. Rev. B* **75**, 125425 (2007).
- <sup>34</sup>Yu. V. Skrypnik and V. M. Loktev, *Phys. Rev. B* **75**, 245401 (2007).
- <sup>35</sup>P. J. Hirschfeld and W. A. Atkinson, *J. Low Temp. Phys.* **126**, 881 (2002).
- <sup>36</sup>T. Stauber, N. M. R. Peres, and A. K. Geim, *Phys. Rev. B* **78**, 085432 (2008).
- <sup>37</sup>V. Mujica, M. Kemp, and M. A. Ratner, *J. Chem. Phys.* **101**, 6849 (1994).
- <sup>38</sup>T. Fukuda, H. Oymak, and H. P. Jongbae, *Phys. Rev. B* **75**, 195428 (2007); *J. Phys.: Condens. Matter* **20**, 055207 (2008).
- <sup>39</sup>K. S. Dy, Shi-Yu Wu, and T. Spratlin, *Phys. Rev. B* **20**, 4237 (1979).
- <sup>40</sup>John Tomfohr and Otto F. Sankey, *J. Chem. Phys.* **120**, 1542 (2004).
- <sup>41</sup>N. M. R. Peres, T. Stauber, and J. M. B. Lopes dos Santos, *Phys. Rev. B* **79**, 035107 (2009).
- <sup>42</sup>C. Caroli, R. Combescot, P. Nozieres, and D. Saint-James, *J. Phys. C* **4**, 916 (1971); **4**, 2598 (1971); **5**, 21 (1972).
- <sup>43</sup>David K. Ferry and Stephen M. Goodnick, *Transport in Nanostructures* (Cambridge University Press, Cambridge, 2001).
- <sup>44</sup>Hartmut Haug and Antti-Pekka Jauho, *Quantum Kinetics in Transport and Optics of Semiconductors*, 2nd ed. (Springer, Berlin, 2008).
- <sup>45</sup>Abhishek Dhar and Diptiman Sen, *Phys. Rev. B* **73**, 085119 (2006).
- <sup>46</sup>Carlo Beenakker and Christian Schönenberger, *Phys. Today* **56** (5), 37 (2003).
- <sup>47</sup>Ya. M. Blanter and M. Büttiker, *Phys. Rep.* **336**, 1 (2000).
- <sup>48</sup>S. Latil, S. Roche, D. Mayou, and J.-C. Charlier, *Phys. Rev. Lett.* **92**, 256805 (2004).
- <sup>49</sup>Vitor M. Pereira, J. M. B. Lopes dos Santos, and A. H. Castro Neto, *Phys. Rev. B* **77**, 115109 (2008).